



IJOER
RESEARCH JOURNAL

ISSN
2395-6992

International Journal of Engineering Research & Science

www.ijoer.com
www.adpublications.org

Volume-6! Issue-11! November, 2020 www.ijoer.com ! info@ijoer.com

Preface

We would like to present, with great pleasure, the inaugural volume-6, Issue-11, November 2020, of a scholarly journal, *International Journal of Engineering Research & Science*. This journal is part of the AD Publications series *in the field of Engineering, Mathematics, Physics, Chemistry and science Research Development*, and is devoted to the gamut of Engineering and Science issues, from theoretical aspects to application-dependent studies and the validation of emerging technologies.

This journal was envisioned and founded to represent the growing needs of Engineering and Science as an emerging and increasingly vital field, now widely recognized as an integral part of scientific and technical investigations. Its mission is to become a voice of the Engineering and Science community, addressing researchers and practitioners in below areas

Chemical Engineering	
Biomolecular Engineering	Materials Engineering
Molecular Engineering	Process Engineering
Corrosion Engineering	
Civil Engineering	
Environmental Engineering	Geotechnical Engineering
Structural Engineering	Mining Engineering
Transport Engineering	Water resources Engineering
Electrical Engineering	
Power System Engineering	Optical Engineering
Mechanical Engineering	
Acoustical Engineering	Manufacturing Engineering
Optomechanical Engineering	Thermal Engineering
Power plant Engineering	Energy Engineering
Sports Engineering	Vehicle Engineering
Software Engineering	
Computer-aided Engineering	Cryptographic Engineering
Teletraffic Engineering	Web Engineering
System Engineering	
Mathematics	
Arithmetic	Algebra
Number theory	Field theory and polynomials
Analysis	Combinatorics
Geometry and topology	Topology
Probability and Statistics	Computational Science
Physical Science	Operational Research
Physics	
Nuclear and particle physics	Atomic, molecular, and optical physics
Condensed matter physics	Astrophysics
Applied Physics	Modern physics
Philosophy	Core theories

Chemistry	
Analytical chemistry	Biochemistry
Inorganic chemistry	Materials chemistry
Neurochemistry	Nuclear chemistry
Organic chemistry	Physical chemistry
Other Engineering Areas	
Aerospace Engineering	Agricultural Engineering
Applied Engineering	Biomedical Engineering
Biological Engineering	Building services Engineering
Energy Engineering	Railway Engineering
Industrial Engineering	Mechatronics Engineering
Management Engineering	Military Engineering
Petroleum Engineering	Nuclear Engineering
Textile Engineering	Nano Engineering
Algorithm and Computational Complexity	Artificial Intelligence
Electronics & Communication Engineering	Image Processing
Information Retrieval	Low Power VLSI Design
Neural Networks	Plastic Engineering

Each article in this issue provides an example of a concrete industrial application or a case study of the presented methodology to amplify the impact of the contribution. We are very thankful to everybody within that community who supported the idea of creating a new Research with IJOER. We are certain that this issue will be followed by many others, reporting new developments in the Engineering and Science field. This issue would not have been possible without the great support of the Reviewer, Editorial Board members and also with our Advisory Board Members, and we would like to express our sincere thanks to all of them. We would also like to express our gratitude to the editorial staff of AD Publications, who supported us at every stage of the project. It is our hope that this fine collection of articles will be a valuable resource for *IJOER* readers and will stimulate further research into the vibrant area of Engineering and Science Research.



Mukesh Arora
(Chief Editor)

Board Members

Mukesh Arora (Editor-in-Chief)

BE(Electronics & Communication), M.Tech(Digital Communication), currently serving as Assistant Professor in the Department of ECE.

Prof. Dr. Fabricio Moraes de Almeida

Professor of Doctoral and Master of Regional Development and Environment - Federal University of Rondonia.

Dr. Parveen Sharma

Dr Parveen Sharma is working as an Assistant Professor in the School of Mechanical Engineering at Lovely Professional University, Phagwara, Punjab.

Prof.S.Balamurugan

Department of Information Technology, Kalaignar Karunanidhi Institute of Technology, Coimbatore, Tamilnadu, India.

Dr. Omar Abed Elkareem Abu Arqub

Department of Mathematics, Faculty of Science, Al Balqa Applied University, Salt Campus, Salt, Jordan, He received PhD and Msc. in Applied Mathematics, The University of Jordan, Jordan.

Dr. AKPOJARO Jackson

Associate Professor/HOD, Department of Mathematical and Physical Sciences, Samuel Adegboyega University, Ogwa, Edo State.

Dr. Ajoy Chakraborty

Ph.D.(IIT Kharagpur) working as Professor in the department of Electronics & Electrical Communication Engineering in IIT Kharagpur since 1977.

Dr. Ukar W.Soelistijo

Ph D , Mineral and Energy Resource Economics, West Virginia State University, USA, 1984, Retired from the post of Senior Researcher, Mineral and Coal Technology R&D Center, Agency for Energy and Mineral Research, Ministry of Energy and Mineral Resources, Indonesia.

Dr. Samy Khalaf Allah Ibrahim

PhD of Irrigation &Hydraulics Engineering, 01/2012 under the title of: "Groundwater Management Under Different Development Plans In Farafra Oasis, Western Desert, Egypt".

Dr. Ahmet ÇİFCİ

Ph.D. in Electrical Engineering, Currently Serving as Head of Department, Burdur Mehmet Akif Ersoy University, Faculty of Engineering and Architecture, Department of Electrical Engineering (2015-...)

Dr. Mohamed Abdel Fatah Ashabrawy Moustafa

Ph.D. in Computer Science - Faculty of Science - Suez Canal University University, 2010, Egypt.

Assistant Professor Computer Science, Prince Sattam bin AbdulAziz University ALkharj, KSA.

Dr. Heba Mahmoud Mohamed Afify

Ph.D degree of philosophy in Biomedical Engineering, Cairo University, Egypt worked as Assistant Professor at MTI University.

Dr. Aurora Angela Pisano

Ph.D. in Civil Engineering, Currently Serving as Associate Professor of Solid and Structural Mechanics (scientific discipline area nationally denoted as ICAR/08—"Scienza delle Costruzioni"), University Mediterranea of Reggio Calabria, Italy.

Dr. Faizullah Mahar

Associate Professor in Department of Electrical Engineering, Balochistan University Engineering & Technology Khuzdar. He is PhD (Electronic Engineering) from IQRA University, Defense View, Karachi, Pakistan.

Dr. S. Kannadhasan

Ph.D (Smart Antennas), M.E (Communication Systems), M.B.A (Human Resources).

Dr. Christo Ananth

Ph.D. Co-operative Networks, M.E. Applied Electronics, B.E Electronics & Communication Engineering Working as Associate Professor, Lecturer and Faculty Advisor/ Department of Electronics & Communication Engineering in Francis Xavier Engineering College, Tirunelveli.

Dr. S.R.Boselin Prabhu

Ph.D, Wireless Sensor Networks, M.E. Network Engineering, Excellent Professional Achievement Award Winner from Society of Professional Engineers Biography Included in Marquis Who's Who in the World (Academic Year 2015 and 2016). Currently Serving as Assistant Professor in the department of ECE in SVS College of Engineering, Coimbatore.

Dr. Maheshwar Shrestha

Postdoctoral Research Fellow in DEPT. OF ELE ENGG & COMP SCI, SDSU, Brookings, SD
Ph.D, M.Sc. in Electrical Engineering from SOUTH DAKOTA STATE UNIVERSITY, Brookings, SD.

Zairi Ismael Rizman

Senior Lecturer, Faculty of Electrical Engineering, Universiti Teknologi MARA (UiTM) (Terengganu) Malaysia
Master (Science) in Microelectronics (2005), Universiti Kebangsaan Malaysia (UKM), Malaysia. Bachelor (Hons.) and Diploma in Electrical Engineering (Communication) (2002), UiTM Shah Alam, Malaysia

Dr. D. Amaranatha Reddy

Ph.D.(Postdoctoral Fellow,Pusan National University, South Korea), M.Sc., B.Sc. : Physics.

Dr. Dibya Prakash Rai

Post Doctoral Fellow (PDF), M.Sc.,B.Sc., Working as Assistant Professor in Department of Physics in Pachhungga University College, Mizoram, India.

Dr. Pankaj Kumar Pal

Ph.D R/S, ECE Deptt., IIT-Roorkee.

Dr. P. Thangam

BE(Computer Hardware & Software), ME(CSE), PhD in Information & Communication Engineering, currently serving as Associate Professor in the Department of Computer Science and Engineering of Coimbatore Institute of Engineering and Technology.

Dr. Pradeep K. Sharma

PhD., M.Phil, M.Sc, B.Sc, in Physics, MBA in System Management, Presently working as Provost and Associate Professor & Head of Department for Physics in University of Engineering & Management, Jaipur.

Dr. R. Devi Priya

Ph.D (CSE),Anna University Chennai in 2013, M.E, B.E (CSE) from Kongu Engineering College, currently working in the Department of Computer Science and Engineering in Kongu Engineering College, Tamil Nadu, India.

Dr. Sandeep

Post-doctoral fellow, Principal Investigator, Young Scientist Scheme Project (DST-SERB), Department of Physics, Mizoram University, Aizawl Mizoram, India- 796001.

Mr. Abilash

MTech in VLSI, BTech in Electronics & Telecommunication engineering through A.M.I.E.T.E from Central Electronics Engineering Research Institute (C.E.E.R.I) Pilani, Industrial Electronics from ATI-EPI Hyderabad, IEEE course in Mechatronics, CSHAM from Birla Institute Of Professional Studies.







Mr. Varun Shukla

M.Tech in ECE from RGPV (Awarded with silver Medal By President of India), Assistant Professor, Dept. of ECE, PSIT, Kanpur.

Mr. Shrikant Harle

Presently working as a Assistant Professor in Civil Engineering field of Prof. Ram Meghe College of Engineering and Management, Amravati. He was Senior Design Engineer (Larsen & Toubro Limited, India).

Table of Contents

S.No	Title	Page No.
1	Hydrogen Production System using a Plasma Reactor Authors: Lukáš Tóth, Tomáš Brestovič, Natália Jasminská, Marián Lázár, Romana Dobáková  DOI: https://dx.doi.org/10.5281/zenodo.4297130  DIN Digital Identification Number: IJOER-NOV-2020-1	01-05
2	Vehicle Re-Identification Based on the Authenticity of Orthographic Projection Authors: Qiang Lu, Fengwei Quan, Mingkai Qiu, Xiyang Li  DOI: https://dx.doi.org/10.5281/zenodo.4297136  DIN Digital Identification Number: IJOER-NOV-2020-2	06-16
3	Design and Strength Analysis of the Base for Robot Baxter Authors: Filip Duda, Natália Jasminská, Ingrid Delyová  DOI: https://dx.doi.org/10.5281/zenodo.4297142  DIN Digital Identification Number: IJOER-NOV-2020-3	17-21

Hydrogen Production System using a Plasma Reactor

Lukáš Tóth¹, Tomáš Brestovič², Natália Jasminská³, Marián Lázár⁴, Romana Dobáková⁵

Department of Power Engineering, Faculty of Mechanical Engineering, Technical university of Košice, Vysokoškolská 4, 042 00 Košice, Slovakia

Abstract— The present article deals with a potential to interconnect the plasma technology of waste processing with the technology of hydrogen separation from syngas using metal hydride alloys. It also describes key components of the system used for syngas cleaning and their succession.

Keywords— hydrogen, plasma reaktor, waste treatment, gasification.

I. INTRODUCTION

Conventional procedures of hydrogen recovery are not environment-friendly or require a significant amount of energy. One of the environment-friendly methods of hydrogen recovery is hydrogen separation from syngas produced either as a result of biological processes in microorganisms or as a by-product of technological processing of waste, in particular the gasification technology or waste disposal using plasma reactors. At present, a system of hydrogen recovery from such syngas represents a challenge which is only manageable by a few methods which are costly, technologically demanding or time-consuming.

II. THE PLASMA GASIFICATION PRINCIPLE

Plasma arc gasification is a waste-treatment technology based on the principle of producing a plasma arc discharge mostly from a stream of inert gas (argon, nitrogen etc.). With the use of a high-intensity electric field, plasma-forming gas is transformed into plasma. High temperatures along the edges of the plasma arc discharge ensure a stable heat flow required for the thermal decomposition of waste. Due to the effect of high dissociation energy, the organic component of the waste is decomposed into simple gas molecules. Inorganic waste components, in form of liquid slag and an alloy of metals, are accumulated in the lower part of the reactor and periodically discharged through tap holes.

Depending on the percentages of contained combustible components, including mainly hydrogen and carbon monoxide, syngas may be used, after the cooling and cleaning phases, for energy purposes through combustion in incineration plants [1].

An input material for plasma gasification is waste, including biological waste, communal waste, sledge from waste water treatment plants, hazardous waste from hospitals and healthcare facilities, or certain types of waste from production.

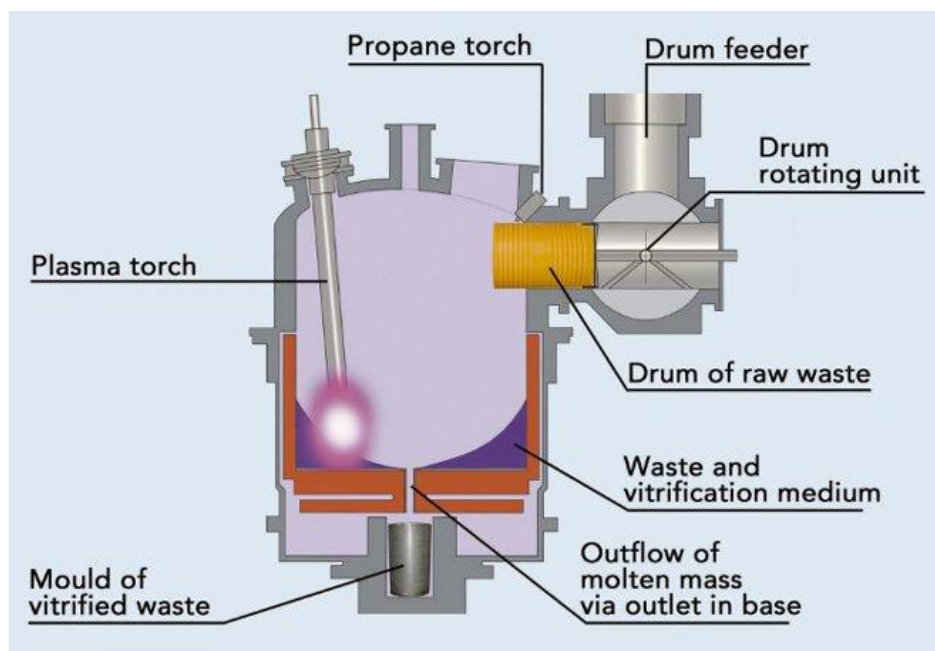


FIGURE 1: Basic system of plasma reactor [3]

First of all, the waste must be subjected to technological treatment. In order to become suitable for processing, the waste must meet certain technological parameters required for individual reactor types. In the case of biological waste and sledge from waste water treatment plants, it must be dried, and only then it may be processed similarly to processing any other waste, i.e. by crushing and granulating. This method is used to create a more compact homogeneous mixture which is easier to handle and improves the regulation of inserting charges into a plasma reactor. After the waste is processed into a size that is easier to handle, it is charged into the reactor. This is carried out using a special feeding device which inserts charges into the plasma reactor where the material decomposes.

The electrical current passes through electrodes, creating an arc between them or between the electrode and the reactor bottom. The most frequently used plasma-forming gas is nitrogen, due to its good accessibility, and in a high-intensity electric field it transforms into plasma.

III. SYNGAS CLEANING SYSTEM

Thermal Syngas generated during a thermal process must be cleaned of undesired components. The cleaning process consists of several phases aimed at preparing syngas for hydrogen separation using metal hydride alloys. The cleaning phases are as follows:

- Removal of particulate matter;
- Removal of acids;
- Removal of oxygen; and
- Removal of present water in form of vapour or aerosol.

3.1 Removal of particulate matter

In terms of waste processing in a plasma reactor, particulate matter may be divided into 3 basic categories:

- Coarse particles PM10 – particles with a diameter of 10 micrometres or less – these particles may easily pass to the lung tissues where they settle and cause health problems;
- Fine particles PM2.5 – particles with a diameter of 2.5 micrometres or less – they have multiple negative effects on human health, primarily affect the airways;
- Particles larger than 10 micrometers.

In practice, particulate matter is separated using devices for particulate matter separation which are based on the principle of separating particles of pollutants from a stream of gas passing through the separator surfaces (either directly onto the separator wall, for example in gravity or cyclonic separators, or inside a separator, for example in electric or rotary separators). In most separators, particulate matter must be removed from the separator surfaces, either continuously or in certain time intervals, while the filter regenerates [2].

Particulate matter removal devices operate on one of the key separation principles:

- Gravity principle – e.g. a louvered separator – using gravity forces;
- Inertia principle – e.g. a cyclonic separator or a fan separator;
- Electrostatic principle – using Coulomb force, with the efficiency as much as 99.99 %;
- Diffusion principle – forces of molecular origin induce diffusion of particles, applicable to particles smaller than 1 μm ;
- Interception principle – particles moving near the separation surface may separate through it thanks to their final size; and
- Centrifuge principle – the movement of particles towards the separator surfaces is induced by the centrifugal force.

Considering the above listed physical principles, particulate matter separators are categorised as follows:

- Dry mechanical separators – dry separation;
- Wet mechanical separators – wet separation;

- Filters;
- Electrostatic separators.

3.2 Removal of acid

Waste treatment is a process in which it is impossible to avoid the presence of certain substances, for example sulphur, chlorine etc., which may interact with other present elements, such as hydrogen or oxygen, with the result of forming acids. These acids represent a significant risk either for the environment into which they may be released, or primarily for metal hydride alloys from which hydrogen will be separated from the remaining syngas components. The effect of such acids is extreme degradation of metal hydride alloys, and in some alloys there is a potential of formation of hazardous or toxic substances which may be released into the environment and contaminate it.

One of the most probable products of reactions in the event of a higher percentage of sulphur, with regard to an excessive content of H_2 and O_2 -deficient atmosphere, is H_2S . Although it is not an acid, it is extremely toxic [4].

During the dry processes of desulphurisation, hydrogen sulphide is absorbed and decomposed into sulphuric acid or elementary sulphur. These processes exhibit a lower potential of removing hydrogen sulphide, but they do not require supplying air to the system or use toxic catalysers.

This process is very slow when the sulphur content in the gas is high. In the case of production of syngas with a low content of sulphur, the application of a desulphurisation system based on dry processes is possible; however, if the sulphur content is high, this process is unsuitable. The desulphurisation process is described by the following equation:



Following the saturation, the material may be regenerated as described by the following equation:



IV. SYSTEM OF INTERCONNECTING A PLASMA REACTOR WITH A MH SEPARATOR

With regard to the efforts aimed at hydrogen recovery by separation from syngas produced in a plasma reactor, syngas must be cleaned, as described above, or otherwise treated; sometimes even the equipment to be used for such treatment must be adjusted. The whole system should consist of a set of successive devices which will remove all undesired substances from syngas. A basic scheme is shown in Fig. 2.

After the particulate matter and acid gases are removed from syngas, oxygen must be removed from the gas stream, as it is an important contaminant which may damage or even completely deteriorate metal hydride alloys; as a result, this would put the metal hydride separator out of service. For the purpose of oxygen removal, in this case it is more appropriate to let it react with the present oxygen, with the result of producing water in the presence of catalyser – palladium. This method facilitates reduction of the oxygen content in syngas down to dozens of ppm. However, this may result in a partial increase in humidity in the gas.

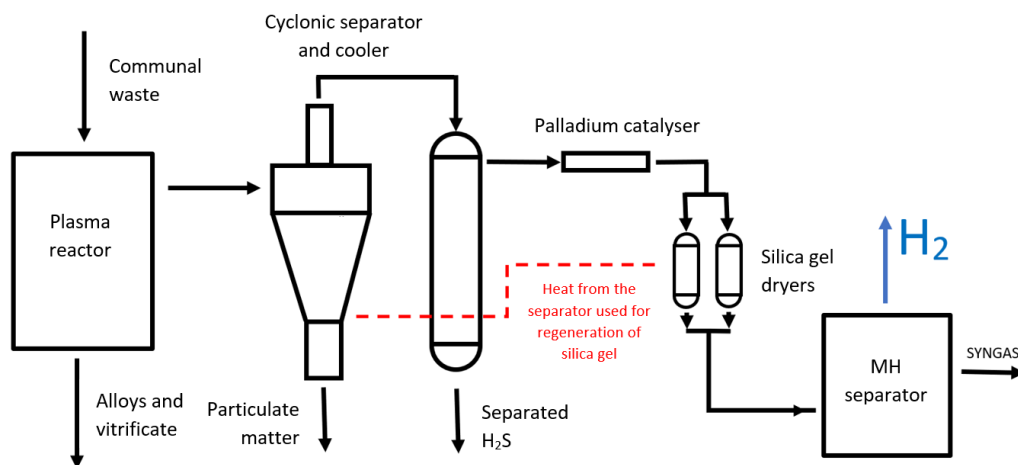


FIGURE 2: Basic system of connection plasma reactor with MH separator

V. METAL HYDRIDE SEPARATOR OF HYDROGEN

Hydrogen separation from syngas may be carried out while applying several methods, mostly based on the principle of membrane separation of individual components. However, such separation puts high requirements on the membrane production technology and service life. An interesting alternative may be the use of metal hydride alloys which are able to absorb hydrogen into their intermetallic structures; this facilitates efficient hydrogen separation from the remaining syngas components.

5.1 MH separator principle

A separator is a simple device consisting of a set of electromagnetic valves, pressure meters, pressure vessels and heating/cooling devices. A basic separator scheme is shown in Fig. 3.

Gas from a plasma reactor enters the system in the mixing feeder zone. In the scheme, the inlet from a plasma reactor is replaced with a mixing feeder for initial experiments in which a constant syngas mixture will be used, unlike the gas produced in a plasma reactor, because in that case the syngas composition continuously changes, depending on the waste composition and quantity.

Gas pressure is measured using a digital manometer before it enters the separator. Behind the electromagnetic valve which facilitates the supply of syngas into the system, there is a reduction valve which prevents a sudden pressure increase in the system.

Following a regulated entry into the system, syngas passes into a metal hydride separator where hydrogen is stored into the intermetallic structure of a metal. As hydrogen storage is an exothermic reaction, the container must be cooled to prevent overheating. The container is cooled by the system of Peltier thermocouples which are able, thanks to electrical energy, to heat up one side while cooling down the other side of the container. The heated side must be then cooled down by the system of water processor coolers which are able to prevent overheating of that side above the maximum operating temperature of the Peltier thermocouple. After certain period of time defined by the software, the inlet piping closes and stops the gas supply to the separator. Using a digital manometer located near the pressure vessel, changes in pressure are measured. Such changes are caused by storing hydrogen in the alloy. As soon as the pressure decrease in the separator system stops, it is possible to conclude that there is no hydrogen left in the system or that the alloy has been fully saturated.

When the alloy is saturated, the remaining syngas components are withdrawn. The first phase consists of releasing the overpressure using the electromagnetic valve and the reduction piping. Subsequently, after the pressure decreases down to approximately 0.1 to 0.3 bars, the electromagnetic valve closes and the remaining syngas is exhausted using a vacuum pump.

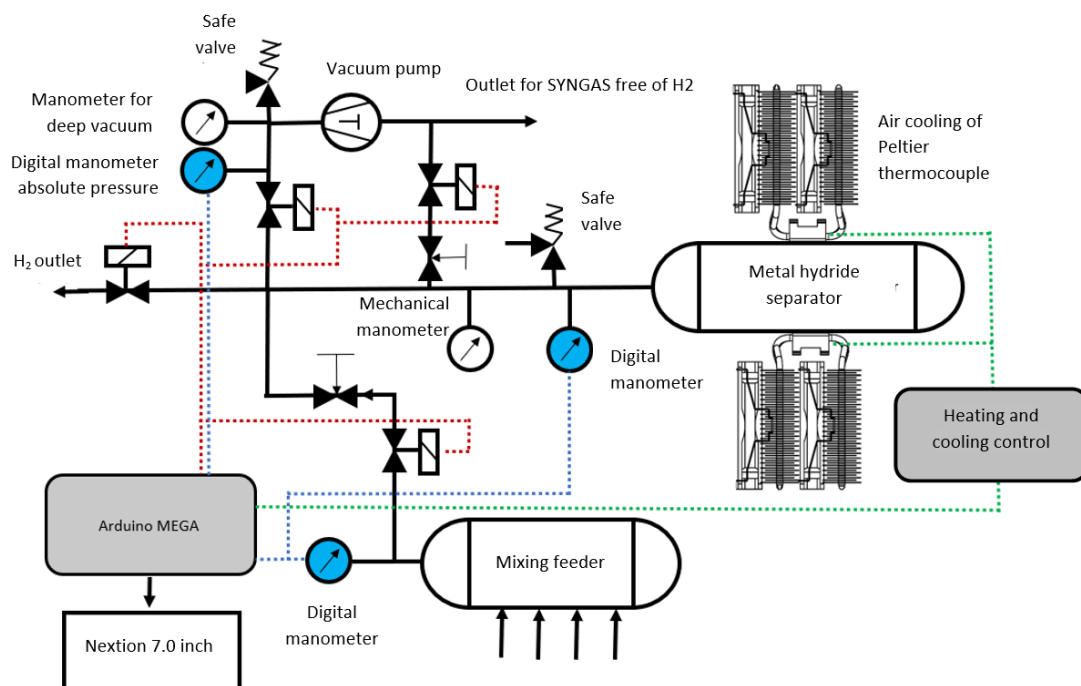


FIGURE 3: System of MH separator

In the vacuum pump area, there are digital and mechanic manometers for absolute pressure which is also able to measure deep vacuum.

The exhaust time must not exceed the period determined on the basis of the measured properties of individual alloys, due to subsequent exhaust of hydrogen from the alloy. In order to prevent this, exhaust of the remaining components must not exceed the shortest necessary period. Following the exhaust, hydrogen is forced out of the alloy. For this purpose, the alloy must be heated up to the operating temperature. That is when the polarity of Peltier thermocouples is reversed, i.e. the surface which was cooled down during hydrogen storage is now heated up, and vice versa. Heating causes hydrogen desorption and a pressure increase. After the pressure is increased to a certain value determined according to predefined conditions related to the operating conditions of the alloys and the required conditions at the hydrogen outlet from the system, electromagnetic valves open and hydrogen is let into the system for further processing.

VI. CONCLUSION

The measurement system described in the article will soon be subjected to the construction and testing phase while the emphasis will be put mostly on testing the resistance of metal hydride alloys to acids produced during the thermal decomposition of communal waste. Furthermore, alloys will be tested for their resistance to CO and CH₄ and the effects of alloys on a potential decomposition of these substances.

ACKNOWLEDGEMENTS

Acknowledgments: This paper was written with the financial support of the granting agency VEGA within the project solution No. 1/0108/19 and No. 1/0626/20 and of the granting agency KEGA within the project solution No. 005TUKE-4/2019.

REFERENCES

- [1] LÁZÁR, M., BRESTOVIČ, T., ČARNOGURSKÁ, M.: Vysokoteplotné technológie spracovania odpadu. In: Košice, 2018, ISBN 978 80 553 2756 3.
- [2] ENVIROPORTAL. Tuhé znečisťujúce látky a spôsob ich odstraňovania zo životného prostredia. Dostupná na: <<https://www.enviroportal.sk/clanok/tuhe-zneclistujuce-latky-a-sposob-ich-odstranovania-zo-zivotneho-prostredia>>.
- [3] ZWILAG. Plasma plant. Dostupné na <https://www.zwilag.ch/en/plasma-plant-_content---1--1047.html>.
- [4] STRAKA, F., kol.: Bioplyn. Praha, 2006, ISBN 807328 096.

Vehicle Re-Identification Based on the Authenticity of Orthographic Projection

Qiang Lu¹, Fengwei Quan², Mingkai Qiu³, Xiyang Li^{4*}

^{1,2,3,4}Guangdong Provincial Key Laboratory of Intelligent Transportation Systems

^{1,2,3,4}School of Intelligent Systems Engineering, Sun Yat-sen University, Guangzhou Guangdong 510006, China

*Corresponding author at: Research Center of Intelligent Transportation System, School of Engineering, Sun Yat-sen University, Guangzhou, Guangdong, 510006, China

Abstract— *Vehicle re-identification is still a problem do not receive much attention in the multimedia and vision communities. Since most existing approaches mainly focus on the overall vehicle appearance for re-identification and do not consider the visual appearance changes of sides of vehicle, called local deformation. In this paper, we propose a vehicle re-identification method based on the authenticity of orthographic projection, in which three sides of vehicle are extracted, and the local deformation is explicitly minimized by scaling each pair of corresponding side to uniform size before computing similarity. To compute the similarity between two vehicle images, we 1) construct 3D bounding boxes around the vehicles, 2) extract sub-images of the three sides of each vehicle like a three-view drawing, 3) compute the similarity between each pair of corresponding side sub-images, and 4) use their weighted mean as the final measure of similarity. After computing the similarity between the query vehicle and all candidate vehicles, we rank these similarities and take the vehicle with the maximum similarity as the best match. To evaluate this approach, we use a dataset with 240 pairs of vehicle images extracted from surveillance videos shot at seven locations in different directions. The experimental results show that our proposed method can achieve 75.83% matching accuracy for the top-1 ranked vehicle and 91.25% accuracy for the top-5 vehicles.*

Keywords— *3D bounding boxes, local deformation, vehicle re-identification, weighted mean.*

I. INTRODUCTION

Vehicle re-identification refers to the problem of identifying a query vehicle in a gallery of candidates captured from non-overlapping cameras. As the development of smart city, how to research a given vehicle in a large-scale surveillance video data is an emerging and important problem that should pay more attention. Unlike person re-identification [1,2,3] which attract widespread attention, researches on vehicle re-identification are still limited. In vehicle-related research, the major researches in the multimedia and computer vision fields are focus on vehicle detection [4], fine-grained recognition [5] and driver behavior modeling [6]. Different with vehicle fine-grained recognition, which aims at recognizing the model of a given vehicle, vehicle re-identification is a more challenging task since there exist many vehicles share the same model and they should be identified as different classes.

As each vehicle's license plate number is unique, vehicle re-identification may not difficult if the license plate number can be distinguished [7,8,9]. However, in real-world applications, especially in most surveillance videos, license plates cannot be clear enough to identify a vehicle due to the influences of camera distance and resolution. Therefore, license plate number matching is not a reliable method of re-identification. Instead, achieving high re-identification accuracy based on vehicle appearance is desired.

Existing re-identification approaches [10,11,12,13] focus on learning an embedding space in which similar images are pulled closer and dissimilar images are pushed far away, and the embedding spaces are optimized by a triplet loss [14], circle loss [15] or other improved triplet losses function. These methods all reduce the intra-class variance between images of same vehicles implicitly, and here we aim to construct a method that could explicit reduce the intra-class variance.

Due to the variations in viewing angle, shooting distance and background clutter, one of the challenges in vehicle re-identification is same vehicle capture from different camera via different views may have significantly different appearance, as shown in Fig. 1. Even after scaling the vehicle images to uniform size, differences in appearance still exist since visual appearance changes of each side of vehicle, called local deformation, is not uniform. So, to minimize the influence of vehicle deformation, we aim to find a method that can deal with local deformation rather than overall deformation, here, overall deformation means visual appearance changes of the whole vehicle.



FIGURE 1: A vehicle captured from different camera viewpoints.

Images captured by orthographic projection can be used for scale- and rotation-invariant detection [16]. By making three-view drawings based on orthographic projection, the real shape of all three directions (front, top and side) can be obtained, which is called the authenticity of orthographic projection. As vehicles can be approximated as rectangular solids, it is possible to construct an approximate three-view drawing of a vehicle by geometric transformation. So, if we can obtain each vehicle’s three views as a three-view drawing and unify the size of each pair of corresponding views (front-to-front, top-to-top and side-to-side), then the deformation of each view can be reduced, and the influence of vehicle deformation minimized. Based on this idea, we propose a vehicle re-identification method based on the authenticity of orthographic projection.



FIGURE 2: 3D bounding box constructed around vehicle, and then split so the three views form a three-view drawing.

Given two images of vehicles, we first construct 3D bounding boxes [17] around them, split each vehicle’s three views like a three-view drawing, as shown in Fig. 2. Then, we unify the size of each pair of corresponding views, compute the three similarities between them and apply a weighting strategy to obtain the final similarity. After computing the similarities between the query vehicle and all candidate vehicles, we sort these similarities and take the vehicle with the maximum similarity to be the query vehicle. The re-identification procedure is as shown in Fig. 3.

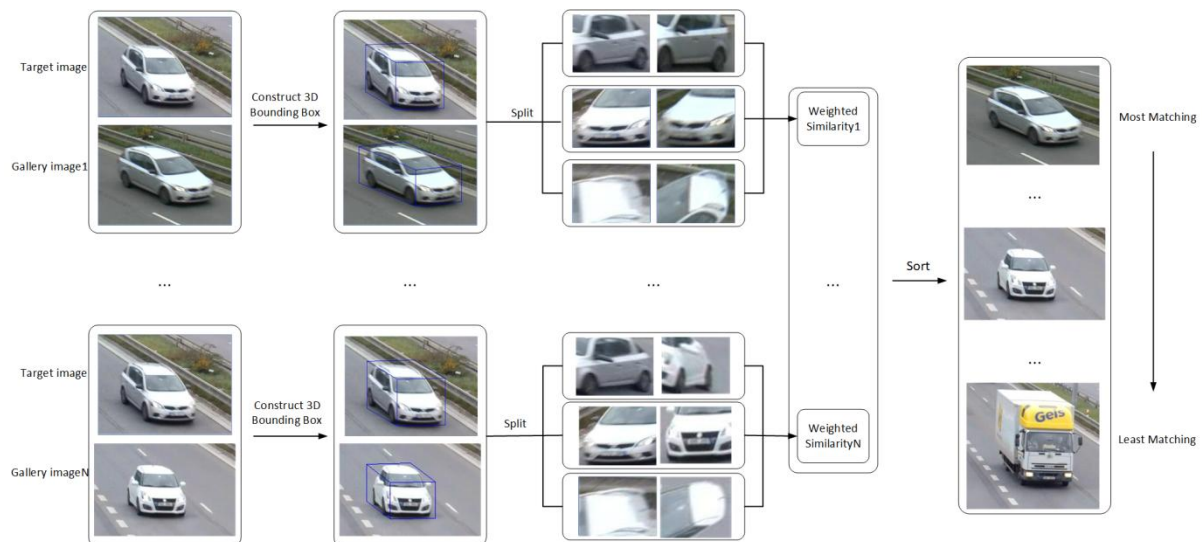


FIGURE 3: Vehicle re-identification method proposed in this paper

The main contribution of this work to the field of vehicle re-identification is that, unlike previous studies, we propose a method that can deal with the deformation of local sides rather than overall deformation. The proposed model can be used to effectively improve the performance of some existing methods in vehicle re-identification or vehicle retrieval.

The remainder of this paper is organized as follows: In Section II, early and recent algorithms for target re-identification are reviewed. In Section III, we explain our proposed method for vehicle re-identification. In Section IV, we describe the datasets used, the evaluation metrics and the experimental results. Finally, in Section V, we conclude our work.

II. RELATED WORK

Like person re-identification, vehicle re-identification is a type of target re-identification. This involves a computer being given an image of a target object from one camera view, then using it to identify an image of a target object from a set of candidates captured from other camera views. As the principle of these two types of target re-identification is basically the same, some methods of person re-identification can be applied to vehicle re-identification.

Person re-identification: The work of person re-identification mainly focus on two parts: 1) developing a robust descriptor to handle variations in appearance, 2) designing an effective distance metric to measure the similarity between images.

The first category of research mainly focuses on developing a discriminative representation that is robust to cross-view appearance variations. Sunderrajan et al. [1] propose a clothing context-aware color extraction method to learn color drift patterns in a non-parametric manner using the random forest distance (RFD) function. Wei et al. [18] develop a pedestrian image descriptor named Global-Local-Alignment Descriptor; this descriptor explicitly leverages the local and global cues in human body to generate a discriminative and robust representation. To promote the results of designing a descriptor, Wang et al [19] design a data-specific adaptive metric method to conquer the zero-shot and fine-grained difficulties in the re-id problem.

The second category of research aims to find a mapping function from the feature space to another distance space where feature vectors from the same target are more similar than those from different ones. Triplet loss or other improved triplet loss is used to model the intra-class variance and inter-class variance. Ding et al. [2] considered the re-identification problem as a ranking issue and used triplet loss to obtain the relative distance between images. Chen et al. [20] designed a quadruplet loss process, which can lead to model outputs with larger inter-class variation and smaller intra-class variation compared with the triplet loss method. Sun et al. [15] propose a circle loss which offers a more flexible optimization approach towards a more definite convergence target.

Except for these two categories, there are also some other researches focus on re-ranking. Leng et al. [3] proposed an automatic bidirectional ranking method based on content and context similarity, the gallery images are treated as new probes to query in the original gallery set. Ye et al. [21] propose a method exploring both similarity and dissimilarity relationship for ranking optimization, the method improve the quasi-similar galleries' ranking orders and penalize the quasi-dissimilar galleries. Sarfraz et al. [22] introduce an expanded cross neighborhood re-ranking method by integrating the cross neighborhood distance. A local blurring re-ranking [23] employs the clustering structure to improve neighborhood similarity measurement, refining the ranking list.

Vehicle re-identification: Some researches focus on doing vehicle re-identification not only by vehicle image, but also with license plate information or spatial-temporal information of the vehicle, Liu et al. [24,25] utilizes vehicle image and license plate feature to do coarse-to-fine vehicle research, then do re-ranking by the spatiotemporal information of vehicle to get a better result. Shen et al. [26] and Jiang et al. [27] also train a network with multi task to learn discriminative representations of vehicle, then use the spatiotemporal information of vehicle to do re-ranking.

However, license plate information and the spatial-temporal information always cannot obtain in unconstrained surveillance environment, so, develop a general model only based on visual appearance is more desired.

Similar to person re-identification, vision-based vehicle re-identification methods focus on learning discriminative and robust feature representations. These methods train a multi-task network to extract features, use triplet loss, contrastive loss or other improved triplet loss to model inter-class or intra-class variance. Li et al. [10] designed a multi-task training network including identification, attribute recognition, verification and triplet tasks, and used the element-wise absolute difference of extracted features as the similarity score. Zhu et al. [11, 28] design a hybrid similarity learning function to compute the similarity score, this hybrid similarity is computed by simultaneously projecting the element-wise absolute difference and multiplication of the corresponding deep learning feature pair with a group of learned weight coefficients. Liu et al. [12] design a coupled cluster loss to make the training phase more stable and accelerate the convergence speed. Bai et al. [29] design a group-sensitive-triplet embedding to model intra-class and inter-class variance in learning representation, images of vehicle are divided into groups, and images of each group are supposed to share similar attributes, in this way, the intra-class

variance are well modeled. He et al. [30] proposed a part-regularized discriminative feature preserving method which enhances the perceptive ability of subtle discrepancies.

Some other researches focus on constructing a descriptive representation containing all-view information to solve the multi-view vehicle re-identification problem. Zhou et al. [13] use GAN to generate all-view features from the visible view's feature, then fuse all the inferred features in different views and adopt the final representation for distance metric learning. Zhou et al [31] propose two architecture: one use only CNN and the other use CNN and LSTM to generate all -view features from single view image.

III. VEHICLE RE-IDENTIFICATION BASED ON THE AUTHENTICITY OF ORTHOGRAPHIC PROJECTION

3.1 3D Bounding Boxes Construction

We construct 3D bounding boxes around vehicles from a single image based on the method proposed in [17]. The vehicle's contour C and three directions, as shown in Fig. 4, are needed for the construction. The first direction V_1 (marked in yellow) is the direction of the traffic. The second direction V_2 (marked in red) is perpendicular to the first direction and parallel to the road. The third direction V_3 (marked in blue) is orthogonal to V_1 and V_2 .

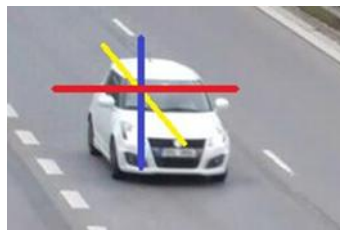


FIGURE 4: The three directions needed for 3D bounding box construction

By quantizing the angle space by bins of 3° from -90° to 90° , which separates the angle space into 60 bins per direction, we transform the regression problem of direction prediction into a classification task. We use Resnet50 [32] with three separate outputs to conduct multi-task prediction of the three directions (see Fig. 5), and use eq. (1) to compute the sum of the cross-entropy of the three predictions as the total loss function for network prediction:

$$Loss = - \sum_{i=0}^2 \sum_{j=0}^{59} y'_{i,j} \log(\hat{y}_{i,j}) \quad (1)$$

Where $y'_{i,j}$ is defined as:

$$y'_{i,j} = \begin{cases} 1, & \text{if truth value of } i^{th} \text{ direction lies in } j^{th} \text{ bin} \\ 0, & \text{otherwise} \end{cases} \quad (2)$$

$y_{i,j}$ is similar to $y'_{i,j}$, but represents the predicted value.

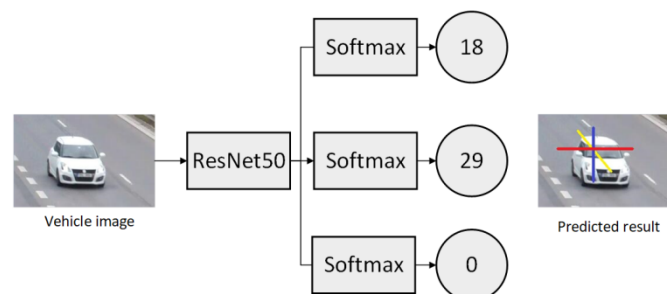


FIGURE 5: Using Resnet50 for prediction of directions. The vehicle image is fed to the network with three separate outputs that predict the angle spaces that its three directions belong to.

For vehicle contour detection, we use the fully convolutional encoder-decoder network designed in [33], which masks with probabilities of vehicle contours for each image pixel (see Fig. 6). To obtain the final contour, we use a different approach to [17], which searches for global maxima along the line segment from the center to the edge points of the 2D bounding box. Here, we only employ binarization to the probability map and use the binary image as the final contour. The reasons we do this simplification are: 1) It will accelerate the whole process. The search process used in [17] will be time-consuming when the 2D bounding boxes are large, as there will be hundreds of lines needed to replicate the search process. In addition, the extra work needed for 2D bounding box estimation is also time-consuming; 2) The difference has a little influence on the re-

identification result. Compared with [17], the final contour will be just a little different in the edge region. In the similarity measure we use, this small difference only has a small effect on the computed similarity and can be ignored.

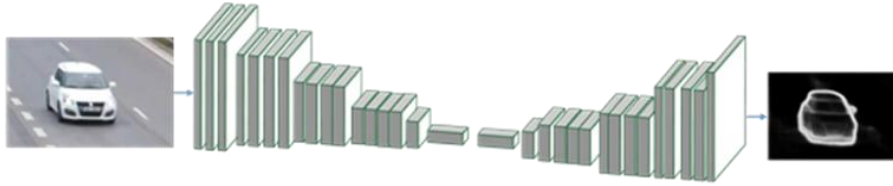


FIGURE 6: Using a fully convolutional encoder-decoder network for estimating vehicle contours

The process of using the vehicle's contour and three directions to construct 3D bounding boxes is as shown in Fig. 7. We put the intersections of each tangent in order, then a 3D bounding box can be obtained by connecting, in order, the seven points: $[(x_A, y_A), (x_B, y_B), (x_C, y_C), (x_D, y_D), (x_E, y_E), (x_F, y_F), (x_G, y_G)]$.

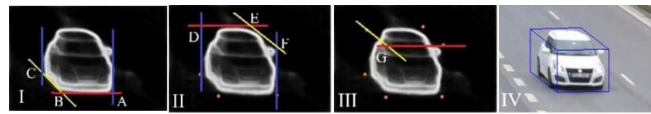


FIGURE 7: Use of a vehicle's three directions and contours to construct a 3D bounding box. (I) Tangent lines and their relevant intersections A, B, C. (II) Derived lines and their intersections E, D, F. (III) Derived lines and intersection G. (IV) Constructed bounding box

3.2 Similarity Measure

The global similarity between two images is calculated after we construct each vehicle's 3D bounding box. All three views of the vehicle—the front, top, and side—are split and the sub-region similarity between each pair of corresponding sides of these two vehicles is computed. Here, we use a simplified deformable diversity similarity (DDIS) method to compute the sub-region similarity.

3.2.1 Deformable Diversity Similarity

DDIS [34] is an algorithm for template matching, which can be used for computing the similarity between two images, and no prior information of the images is needed.

Given two images I_1 and I_2 , let points $p_i, q_j \in \mathbb{R}^d$ represent patches of I_1 and I_2 , respectively. DDIS is used to compute the similarity between two sets of points, $P = \{p_i\}_{i=1}^N$ and $Q = \{q_j\}_{j=1}^M$. Let p^a denote the appearance and p^l the location of patch p (and similarity with q). Find the appearance-based nearest-neighbor (NN) patch p_i for every point q_j s.t. $p_i = \text{NN}^a(q_j, P) = \text{argmin}_{p \in P} d(q_j^a, p^a)$ for a given distance $d(q^a, p^a)$. Let $r_j = d(q_j^l, p_i^l)$ denote the location distance between point q_j and its NN^a . Then, define $k(p_i)$ as the number of patches $q \in Q$ whose NN^a is p_i :

$$k(p_i) = |\{q \in Q: \text{NN}^a(q, P) = p_i\}| \quad (3)$$

Finally, DDIS can be computed as:

$$\text{DDIS}_{Q \rightarrow P} = c \sum_{q_j \in Q} \frac{1}{r_j + 1} \cdot \exp\left(1 - k(\text{NN}^a(q_j, P))\right) \quad (4)$$

where $c=1/\min\{M, N\}$ is a normalization factor.

3.2.2 Simplified Deformable Diversity Similarity (SDDIS)

In our method, we simplify the DDIS according to the actual situation, which is reflected in two ways. 1) We set M as equal to N , where M and N are the numbers of patches of images I_1 and I_2 , respectively. Because scale normalization to the corresponding views is performed, the two corresponding views are of the same size, which means that M equals N . 2) We set $r_j = 0$. Because $1/(r_j + 1)$ is used to quantify deformation in Equation (4), large deformation is given a penalty as r_j is big, so it finds the best and plausible match of a small image within a large image. In our work, we assume that the corresponding views are the best matching sides to each other.

In addition, as we cannot split all three views of the vehicle precisely, the images of some sides will include background or parts of other sides. This means that the location distance between a patch and its nearest-neighbor patch sometimes will be large, even if two images are of the same vehicle. So, the SDDIS similarity measure we use is:

$$SDDIS_{Q \rightarrow P} = \frac{1}{M} \sum_{q_j \in Q} \exp \left(1 - k \left(NN^a(q_j, P) \right) \right) \quad (5)$$

3.2.3 Global Similarity

Given two images—a query image T and candidate image S —let T_f, T_t, T_s be the three views (front, top and side) that are split from the 3D bounding box of T , and similarity for S . After computing all three sub-region similarities between each pair of corresponding views, the global similarity between T and S is calculated as:

$$F(T, S) = W_f \cdot SDDIS(T_f, S_f) + W_t \cdot SDDIS(T_t, S_t) + W_s \cdot SDDIS(T_s, S_s) \quad (6)$$

where W_f, W_t and W_s denote the different weights given to each similarity. Different weights are given because each side has a different influence on the vehicle re-identification process. For example, the front side contains the lights, radiator grille and other discriminative features, which are more useful for distinguishing vehicles than the features of the other sides.

3.3 Vehicle Re-identification (VRID)

In summary, given a query vehicle T , we find the best-matching vehicle amongst a set of gallery candidates $S = \{S_1, \dots, S_n\}$. For n pairs of vehicles $\{T, S_i\}$, we compute their global similarities with the process shown in Fig. 8, sort these n similarities $\{F(T, S_1), \dots, F(T, S_i), \dots, F(T, S_n)\}$, and then the vehicle with the maximum similarity is the best match.

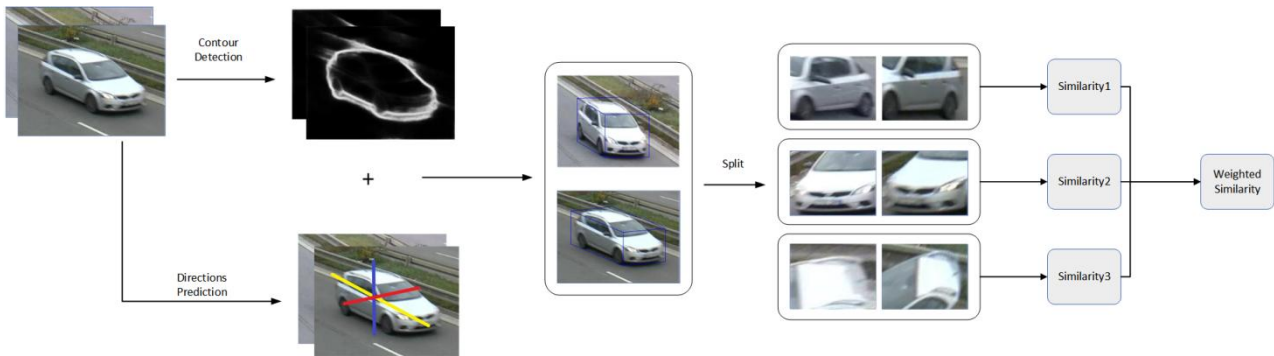


FIGURE 8: Complete process of similarity computing

IV. EXPERIMENTS

4.1 Experiment Dataset

4.1.1 Direction Prediction Dataset

For direction prediction, we used the BOXCAR116K dataset [17] to train the network. BOXCAR116K contains 116,287 images of vehicles shot by 137 cameras. It has annotations for each vehicles' 2D and 3D bounding boxes so we can obtain the required directions from each image by computing the angle between the edges of the 3D bounding boxes and the horizontal line, then take the result to be the ground truth.

4.1.2 Vehicle Re-identification Dataset

For vehicle re-identification, we used the BrnoCompSpeed dataset [35]. It contains 18 full-HD videos, each around 1 h long, captured at six different locations and in three directions for each location. We captured vehicle images manually and paired images of vehicles captured at two different directions. 240 pairs of images were obtained, with examples shown in Fig. 9.

4.2 Experiment Setting and Results

4.2.1 Direction Prediction

After analyzing the BOXCAR116K dataset, we found that direction V_3 was always approximately 90° . Accordingly, we set V_3 to 90° and predicted the other two directions in the experiments.

We trained the Resnet50 network in TensorFlow, added two separate fully-connected layers with *softmax* activation (one for each direction) after the last pooling layer to perform multi-task prediction. We used 96,000 images for training and the other 20,286 images for testing. The prediction accuracy was 89.75% for V_1 and 91.99% for V_2 .



FIGURE 9: Pairs of vehicle images from a vehicle re-identification dataset.

4.2.2 Contour Detection:

For contour detection, we used the model directly pre-trained with the Pascal VOC2007 dataset. Some of the detection results are shown in Fig. 10.



FIGURE 10: Examples of contour detection using the pre-trained model

The images show that the pre-trained contour detection model can acceptably predict a result that completely extracts the vehicle's contour with only a few background pixels incorrectly predicted as contour pixels.

4.2.3 3D Bounding Box Construction

After obtaining the vehicle directions and contours, we constructed 3D bounding boxes following the process shown in Fig.

7. Some of the results are shown in Fig. 11. The method of 3D bounding box construction can create a good result that captures the vehicle's 3D shape. This allows us to split the vehicle's three sides confidently based on the 3D bounding boxes.



FIGURE 11: Examples of 3D bounding box construction

4.2.4 Vehicle Re-identification

As there are few studies on vehicle re-identification, we only compared our method with two others. 1) HOG+LLC, which is a typical method in the field of target re-identification. It first extracts an image's histograms of oriented gradients (HOG) [36], then uses locality-constrained linear coding (LLC) [37] to encode the HOG features, obtains a higher level of image semantic description and, finally, uses the correlation coefficient between the two images' feature vectors as a measure of

their similarity. 2) DDIS. To prove that our method can effectively improve the performance of DDIS, we compared it with the method that directly computes the DDIS between two whole images. Furthermore, to compute the DDIS or SDDIS of two images, we first need to divide the images into patches according to a preset patch size. So, to make comparisons in different patch sizes, the patch size was set to 5, 7, and 9 in the experiment.

In this paper, the evaluation metric is the cumulative matching characteristic curve (CMC) [38], in which the accuracy in k is the probability of observing the correct identity within the top k ranks. The result is shown in Fig. 12 and Table I.

Using the surveillance video dataset, the proposed method achieved 75.83% re-identification accuracy in the top-1 rank and 91.25% accuracy in the top-5 ranks. This proves the feasibility of our approach.

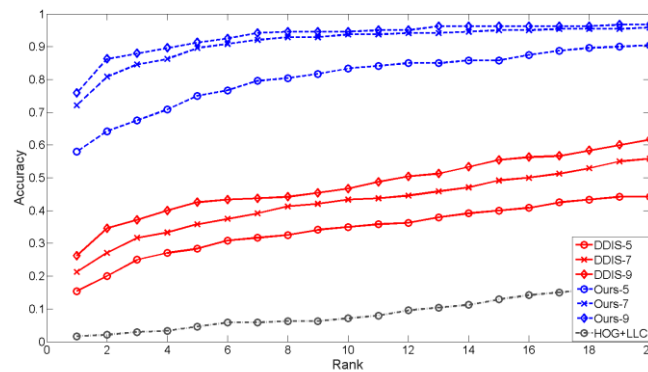


FIGURE 12: Results of vehicle re-identification of 240 pairs of vehicles using our method, the direct DDIS method, and HOG+LLC. The numbers 5, 7, and 9 represent the patch sizes used in SDDIS and DDIS to divide images into patches

TABLE I

COMPARISON OF DIFFERENT VEHICLE RE-IDENTIFICATION METHODS. TOP-K REPRESENTS THE PROBABILITY OF OBSERVING THE CORRECT IDENTITY WITHIN THE TOP K RANKS

Method	Top-1	Top-2	Top-3	Top-4	Top-5
HOG+LLC	0.0167	0.0208	0.0292	0.0333	0.0458
DDIS-5	0.1542	0.2	0.25	0.2708	0.2833
DDIS-7	0.2125	0.2708	0.3167	0.3333	0.3583
DDIS-9	0.2625	0.3458	0.3708	0.4	0.425
Ours-5	0.5792	0.6417	0.675	0.7083	0.75
Ours-7	0.7208	0.8083	0.8458	0.8625	0.8958
Ours-9	0.7583	0.8625	0.8792	0.8958	0.9125

4.3 Analysis

From the experimental results, we can see that our method has much better performance than the HOG+LLC and direct DDIS methods. With the patch size set to 9, our method obtains the best result: the top-1 accuracy is 75.83%, and the top-5 accuracy is 91.25%. Compared with using DDIS directly, our method was 188.9% and 114.7% more accurate, respectively, which proves that it can effectively improve DDIS performance. Both the overall performance and the comparison using DDIS directly prove the feasibility of our method.

The reason why our method can achieve higher accuracy is that it can deal with the deformation of each view rather than just the overall deformation. Just as shown in Fig. 13, the images of a vehicle captured from different camera views have obvious differences in appearance, especially when the images are shot from different sides of the vehicle. Even when we resize the images so that the vehicles are the same size, deformation also exists, so that the differences between images are obvious. In our method, three views of the vehicle are split and scale-normalized to ensure that the vehicle sub-images are the same size. For images shot from different directions, we flipped them. As we can see in Fig. 13, differences in appearances between

images can be minimized by using the process above.



FIGURE 13: Images of a vehicle captured from different camera views, with their three sides split according to 3D bounding boxes. After performing scale-normalization on each corresponding side, differences in the appearance of image pairs can be minimized.

The results indicate that the HOG+LLC method achieved low accuracy. Variation in vehicle orientation and the exclusion of color information may account for this issue.

From the experimental results, the bigger the path size set, the higher the accuracy. This may be because the texture of the vehicle is not complicated. When the patch size is small, many patches in the candidate image may share the same nearest-neighbor patch in the query image as their appearances are similar, which results in a relatively small DDIS value. When the patch size increases, this problem will appear less, so the accuracy will be higher.

V. CONCLUSION

In actual situations, the main differences between images captured from different camera views are differences in scale and image deformation. In order to eliminate these differences, we need a method that can deal with the local deformation of each side of a vehicle, rather than its overall deformation. In this paper, we proposed a method for vehicle re-identification based on the authenticity of orthogonal projection. This means that by making three-view drawings according to orthographic projection, we can obtain the real shape of all three sides of an object. This minimizes scale differences and image deformation.

By splitting vehicle information into three views and flipping the images as required, we can solve the problem presented by

images being shot from different sides. This may provide a feasible way to perform vehicle re-identification when images are shot from different directions, including anterior and posterior views.

A comparison between our method and the direct DDIS method demonstrates the potential of our approach as an auxiliary method for improving the performance of some existing vehicle re-identification methods. Future work will expand this approach to other vehicle re-identification methods, ultimately aiming to build a system suitable for application to expressways.

ACKNOWLEDGEMENTS

This work is supported by Key-Area Research and Development Program of Guangdong Province, No.2020B090921003.

REFERENCES

- [1] S. Sunderrajan and B. Manjunath, "Context-aware hypergraph modeling for re-identification and summarization," *IEEE Transactions on Multimedia*, vol. 18, no. 1, pp. 51–63, 2016.
- [2] S. Ding, L. Lin, G. Wang, and H. Chao. "Deep feature learning with relative distance comparison for person reidentification". *Pattern Recognition*, vol. 48, no. 10, pp. 2993–3003, 2015.
- [3] Q. Leng, R. Hu, C. Liang, Y. Wang and J. Chen, "Bidirectional ranking for person re-identification," 2013 IEEE International Conference on Multimedia and Expo (ICME), San Jose, CA, 2013, pp. 1-6.
- [4] R. S. Feris et al., "Large-Scale Vehicle Detection, Indexing, and Search in Urban Surveillance Videos," *IEEE Transactions on Multimedia*, vol. 14, no. 1, pp. 28-42, Feb. 2012.
- [5] W. Ge, X. Lin, Y. Yu and J. Sochor, "Weakly Supervised Complementary Parts Models for Fine-Grained Image Classification from the Bottom Up," 2019 IEEE Conference on Computer Vision and Pattern Recognition (CVPR), 2019, pp. 3029-3038.
- [6] N. Li, J. J. Jain, and C. Busso, "Modeling of driver behavior in real world scenarios using multiple noninvasive sensors," *IEEE Transactions on Multimedia*, vol. 15, no. 5, pp. 1213–1225, 2013.
- [7] A. R. Selokar and S. Jain, "Automatic number plate recognition system using a fast stroke-based method," *IEEE Transactions on Multimedia*, vol. 1, no. 7, pp. 1-5, Apr. 2014.
- [8] S. Du, M. Ibrahim, M. Shehata and W. Badawy, "Automatic License Plate Recognition (ALPR): A State-of-the-Art Review," in *IEEE Transactions on Circuits and Systems for Video Technology*, vol. 23, no. 2, pp. 311-325, Feb. 2013.
- [9] C. Gou, K. Wang, Y. Yao and Z. Li, "Vehicle License Plate Recognition Based on Extremal Regions and Restricted Boltzmann Machines," *IEEE Transactions on Intelligent Transportation Systems*, vol. 17, no. 4, pp. 1096-1107, April 2016.
- [10] Y. Li, Y. Li, H. Yan and J. Liu, "Deep joint discriminative learning for vehicle re-identification and retrieval," 2017 IEEE International Conference on Image Processing (ICIP), Beijing, 2017, pp. 395-399.
- [11] J. Zhu, H. Zeng, Y. Du, Z. Lei, L. Zheng and C. Cai, "Joint Feature and Similarity Deep Learning for Vehicle Re-identification," *IEEE Access*, vol. 6, pp. 43724-43731, 2018.
- [12] H. Liu, Y. Tian, Y. Wang, L. Pang and T. Huang, "Deep Relative Distance Learning: Tell the Difference between Similar Vehicles," 2016 IEEE Conference on Computer Vision and Pattern Recognition (CVPR), Las Vegas, NV, 2016, pp. 2167-2175.
- [13] Y. Zhou and L. Shao, "Vehicle Re-Identification by Adversarial Bi-Directional LSTM Network," 2018 IEEE Winter Conference on Applications of Computer Vision (WACV), Lake Tahoe, NV, 2018, pp. 653-662.
- [14] F. Schroff, D. Kalenichenko and J. Philbin, "FaceNet: A unified embedding for face recognition and clustering," 2015 IEEE Conference on Computer Vision and Pattern Recognition (CVPR), Boston, MA, 2015, pp. 815-823.
- [15] Y. Sun et al., "Circle Loss: A Unified Perspective of Pair Similarity Optimization," 2020 IEEE Conference on Computer Vision and Pattern Recognition (CVPR), 2020, pp. 6398-6407.
- [16] Jae-Hyeung Park, Joohwan Kim, and ByoungHo Lee, "Three-dimensional optical correlator using a sub-image array," *Optics express*, vol 13, no. 13, pp:5116-5126, 2005.
- [17] J. Sochor, J. Spanhel and A. Herout, "BoxCars: Improving Fine-Grained Recognition of Vehicles Using 3-D Bounding Boxes in Traffic Surveillance," *IEEE Transactions on Intelligent Transportation Systems*. DOI: 10.1109/TITS.2018.2799228.
- [18] L. Wei, S. Zhang, H. Yao, W. Gao and Q. Tian, "GLAD: Global-Local-Alignment Descriptor for Scalable Person Re-Identification," *IEEE Transactions on Multimedia*. DOI: 10.1109/TMM.2018.2870522.
- [19] Z. Wang et al., "Zero-Shot Person Re-identification via Cross-View Consistency," *IEEE Transactions on Multimedia*, vol. 18, no. 2, pp. 260-272, Feb. 2016.
- [20] W. Chen, X. Chen, J. Zhang and K. Huang, "Beyond Triplet Loss: A Deep Quadruplet Network for Person Re-identification," 2017 IEEE Conference on Computer Vision and Pattern Recognition (CVPR), Honolulu, Hawaii, USA, 2017, pp. 1320-1329.
- [21] M. Ye et al., "Person Reidentification via Ranking Aggregation of Similarity Pulling and Dissimilarity Pushing," *IEEE Transactions on Multimedia*, vol. 18, no. 12, pp. 2553-2566, Dec. 2016.
- [22] M. S. Sarfraz, A. Schumann, A. Eberle, and R. Stiefelwagen, "A pose-sensitive embedding for person re-identification with expanded cross neighborhood re-ranking," 2018 IEEE Conference on Computer Vision and Pattern Recognition (CVPR), 2018, pp. 420–429.
- [23] C. Luo, Y. Chen, N. Wang, and Z. Zhang, "Spectral feature transformation for person re-identification," 2019 IEEE International Conference on Computer Vision (ICCV), 2019, pp. 4976–4985.

- [24] X. Liu, W. Liu, H. Ma and H. Fu, "Large-scale vehicle re-identification in urban surveillance videos," 2016 IEEE International Conference on Multimedia and Expo (ICME), Seattle, WA, 2016, pp. 1-6.
- [25] X. Liu, W. Liu, T. Mei and H. Ma, "PROVID: Progressive and Multimodal Vehicle Reidentification for Large-Scale Urban Surveillance," IEEE Transactions on Multimedia, vol. 20, no. 3, pp. 645-658, March 2018.
- [26] Y. Shen, T. Xiao, H. Li, S. Yi and X. Wang, "Learning Deep Neural Networks for Vehicle Re-ID with Visual-spatio-Temporal Path Proposals," 2017 IEEE International Conference on Computer Vision (ICCV), Venice, 2017, pp. 1918-1927.
- [27] N. Jiang, Y. Xu, Z. Zhou and W. Wu, "Multi-Attribute Driven Vehicle Re-Identification with Spatial-Temporal Re-Ranking," 2018 25th IEEE International Conference on Image Processing (ICIP), Athens, Greece, 2018, pp. 858-862.
- [28] Zhu, J., Du, Y., Hu, Y., Zheng, L., and Cai, C. "VRSDNet: vehicle re-identification with a shortly and densely connected convolutional neural network". Multimedia Tools and Applications, 2018, pp. 1-15.
- [29] Y. Bai, Y. Lou, F. Gao, S. Wang, Y. Wu and L. Duan, "Group-Sensitive Triplet Embedding for Vehicle Reidentification," IEEE Transactions on Multimedia, vol. 20, no. 9, pp. 2385-2399, Sept. 2018.
- [30] B. He, J. Li, Y. Zhao and Y. Tian, "Part-Regularized Near-Duplicate Vehicle Re-Identification," 2019 IEEE Conference on Computer Vision and Pattern Recognition (CVPR), 2019, pp. 3992-4000.
- [31] Y. Zhou, L. Liu and L. Shao, "Vehicle Re-Identification by Deep Hidden Multi-View Inference," IEEE Transactions on Image Processing, vol. 27, no. 7, pp. 3275-3287, July 2018.
- [32] K. He, X. Zhang, S. Ren and J. Sun, "Deep Residual Learning for Image Recognition," 2016 IEEE Conference on Computer Vision and Pattern Recognition (CVPR), Las Vegas, NV, 2016, pp. 770-778.
- [33] J. Yang, B. Price, S. Cohen, H. Lee and M. Yang, "Object Contour Detection with a Fully Convolutional Encoder-Decoder Network," 2016 IEEE Conference on Computer Vision and Pattern Recognition (CVPR), Las Vegas, NV, 2016, pp. 193-202.
- [34] Talmi, R. Mechrez and L. Zelnik-Manor, "Template Matching with Deformable Diversity Similarity," 2017 IEEE Conference on Computer Vision and Pattern Recognition (CVPR), Honolulu, Hawaii, USA, 2017, pp. 1311-1319.
- [35] J. Sochor et al., "Comprehensive Data Set for Automatic Single Camera Visual Speed Measurement," in IEEE Transactions on Intelligent Transportation Systems. DOI: 10.1109/TITS.2018.2825609.
- [36] N. Dalal and B. Triggs, "Histograms of oriented gradients for human detection," 2005 IEEE Computer Society Conference on Computer Vision and Pattern Recognition (CVPR'05), San Diego, CA, USA, 2005, pp. 886-893 vol. 1.
- [37] J. Wang, J. Yang, K. Yu, F. Lv, T. Huang and Y. Gong, "Locality-constrained Linear Coding for image classification," 2010 IEEE Computer Society Conference on Computer Vision and Pattern Recognition, San Francisco, CA, 2010, pp. 3360-3367.
- [38] C. Arth, C. Leistner and H. Bischof, "Object Reacquisition and Tracking in Large-Scale Smart Camera Networks," 2007 First ACM/IEEE International Conference on Distributed Smart Cameras, Vienna, 2007, pp. 156-163.

Design and Strength Analysis of the Base for Robot Baxter

Filip Duda¹, Natália Jasminská², Ingrid Delyová³

^{1,2}Department of Power Engineering, Faculty of Mechanical Engineering, Technical university of Košice, Letná 9, 042 00 Košice, Slovakia

³Department of Applied Mechanics and Mechanical Engineering, Faculty of Mechanical Engineering, Technical university of Košice, Letná 9, 042 00 Košice, Slovakia

Abstract— This paper discusses the issue of the subsystem of mobility and solves the design of the lower mobile base for a robot called Baxter. In this paper you can see all the models and parts that are used in construction of mobile base, from which the initial model of the base is created. After making a model of a base, we were putting a load (represents the weight of a robot) on it so we could determine what kind of relative deformations and stresses are created by using finite element method analysis FEM. Later we optimised the base (for example we were changing the length dimensions of some parts), so we could get better results from FEM analysis and also, we wanted the optimised base to acquire similar dimensions and weight as a commercial base. At the end we created technical sheets of all the parts of the base. These technical sheets were later sent to university SIGMA in Clermont-Ferrand (France), from which they constructed mobile base for robot Baxter. FEM analysis was done in program called NX Siemens and models of individual parts were modelled in CATIA V5.

Keywords— mobile base, subsystem of mobility, service robot, Baxter, strength analysis, finite element method.

I. INTRODUCTION

Robots in today's world plays a very important part. General usage of robots is pretty much used everywhere. They are important in many departments such as engineering, medical, food industry or in various manufacturing processes where these robots are compulsory. Some of these robots have to move from one place to another and this can be provided by subsystem of mobility.

Baxter is a robot that resembles humanoid robot but it is service robot that was created and manufactured in company called Rethink robotics and as a start-up and founder of this company is Rodney Brooks. This robot is used for manual repetitive tasks for example storing, loading, retrieving and sorting which means that this robot can later in future replace human in these simple tasks. Baxter is used in many universities as a teaching aid in the classes of robotics, mechanical engineering and also in many IT departments. It is not required to use any safety requirements while using this robot in comparing with other robots. This robot simply stops when something interrupts its working environment. Only disadvantage of Baxter is that it does not have mobile base which means, it cannot move from one place to another.

The purpose of this article is to design subsystem of mobility for this robot. Company that created this robot is already selling commercial mobile base but it is very expensive where the price of this robot is around 40-thousand dollars. University in Clermont-Ferrand decided to create the mobile base for this robot which is going to be cheaper than commercial base and it is also going to have similar properties than commercial base.

First part of this paper is related to design of the mobile base where the first initial model is going to be loaded by the weight of the robot. Generated strain and deformation were calculated by using FEM analysis in NX Siemens. In the beginning of the FEM analysis we had to define materialistic properties to each model of the base. Later we compared these results with analytical results from selected beam of mobile base where we used method of differential equation of the deflection line to solve bending. In order to solve stresses, it was first necessary to determine the static conditions of equilibrium and determine course of bending moment.

Later, the base was changed, but in such a way that the weight and dimensions of the optimised based are approximately the same as the weight and dimensions of commercial mobile base. Weight of the commercial mobile base is around 80 kilograms.

At the end we simulated strength analysis of a wheel to determine relative strain and stress after one turnaround.

After optimising the base, we have chosen the final model of the mobile base. For this final model we created technical sheets that would be used for construction of the base.

II. DESIGN OF THE MOBILE BASE

The whole design of mobile base is simplified, as the robot will move and control on a flat surface and movement of the robot on inclined plane will not be considered. Design does not consider the use of ordinary wheels but the unidirectional wheels (Omni wheels) which compared to ordinary wheels, do not require turning the front wheels or by using auxiliary wheels in order for a robot to turn. These wheels provide the advantage that robot can easily rotate around its own axis.

Another simplification of the design of the mobile base is the fact that the robot stands straight and does not bend, therefore we do not consider the movement of the robot on an inclined plane. The locomotive system of the mobile base for Baxter robot consists of two shafts which are connected by a clutch, one shaft is connected to the motor and the other is connected to the wheel. Information on shafts regarding the dimensions and motors for the mobile base, which were calculated and selected by students at SIGMA University in Clermont-Ferrand (France), was also used for design of the mobile base.

The mobile base consists of two main parts, which are the upper part and lower part of mobile base.

The upper part is used to carry the robot and forms driven axle. In this part it was necessary to create a platform, on which robot will sit. The lower part forms drive axle. At the end we created a support element that connects these two parts together.

The optimised model (Fig.1) of driven axle of a mobile base consists of these parts:

TABLE 1
USED COMPONENTS FOR CONSTRUCTION OF MOBILE BASE

Component	Dimensions (mm)	Quantity
Platform	378x360	1
Aluminium profile	90x90x800	4
Aluminium profile	93x45x680	2
Aluminium profile	93x45x450	4
Aluminium profile	93x45x139	2
Aluminium profile	93x45x216	2
Connector	87x87	8
Connector	35x35	14
Bolt screw	M8	32
Nut	M8	32
Bolt screw	M6	44
Nut	M6	44

The drive axle of the movable base consists of the following main components: protective box, motor, platform (on which the motor is mounted), two shafts, clutch, bearing, wedge, OMNI wheel (unidirectional wheel), connectors (connecting the drive axle to the driven). For the drive axle, it is necessary to distinguish between the left and right side, which differ from each other by the wheel.

Locomotion system of the base consists of two shafts, bearing, clutch, engine and wheel. One of the shafts is connected to the wheel and the other is connected to the engine. As a bearing we used flexible coupling RGS-AL24 with rubber rollers, which connects shafts together. Because of the dimensions of shafts, a double-row ball bearing with angular contact by norm STN 02 4665 was determined. The type of bearing we used A-2Z/C3. As an engine we selected Dynamixel PRO L42-10-S300-R. This type of engine is commonly used as an actuator in many robots. As a wheel we used Mecanum wheel or unidirectional. On this wheel there are external rollers. Each of the rollers has an axis rotation of 45° to the plane of the wheel and 45° to the axis of the axle. The main advantage of these wheels is that robot does not need to turn front wheels in order to change the direction of the robot. Robot can simply rotate on its own axis to change the direction.

Later we optimized the base by changing length dimensions of individual parts of the base with intention that our base must resemble the size and weight of a commercial base.

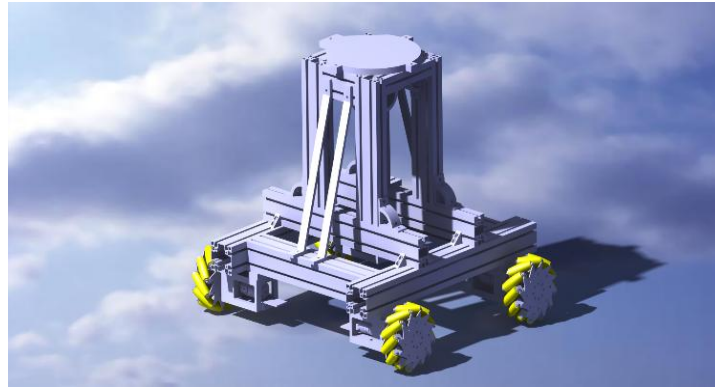


FIGURE 1: Optimized mobile base of a robot Baxter

III. STRENGTH ANALYSIS OF THE BASE

In the first step, it was necessary to convert the model created in the Catia V5 into the NX Siemens, in which strength calculations were performed using finite element method FEM. The total strength analysis can be divided into two parts, where in first part we calculated strength output parameters for the whole structure except for wheel. In the second part we performed strength analysis on the wheel by using quarter model.

3.1 Determination of materials for individual parts

TABLE 2

MECHANICAL PROPERTIES OF USED MATERIALS WHERE Re- YIELD STRENGTH, Rm- TENSILE STRENGTH, μ - POISSON RATIO, ρ - DENSITY, E- YOUNG MODULUS

Material	Re (MPa)	Rm (MPa)	μ	ρ ($\frac{g}{m^3}$)	E (MPa)
Steel 12060	420	750-900	0,3	7,86	$2 \cdot 10^5$
Aluminium steel 6061	276	310	0,33	2,7	$6,89 \cdot 10^4$
Nylon 66	60	85	0,35	1,2	3500

3.2 Determination of boundary conditions

In the first part of strength analysis, it was necessary to determine the connections of the individual parts before the start of the simulation, so the first boundary condition is surface to surface connection. As the second boundary condition we had to define fixed support. The fixed support was defined on the plate of each wheel by which we calculated deformations and stresses on each part of the mobile base except for wheels. Before we could start the simulation, we had to put a loading force generated by weight of the robot on top of the platform of the mobile base. The force is perpendicular to the plane of the platform with around 800N.

TABLE 3

CONDITION SEQUENCES WHERE F_x IS FORCE IN x DIRECTION AND F_z IN z DIRECTION

Condition	Parameters [N]
0-1: 0°	$F_x = 400; F_z = 0,1$
1-2: 45°	$F_x = 283; F_z = 283$
2-3: 90°	$F_x = 0,1; F_z = 400$
3-4: 135°	$F_x = -283; F_z = 283$
4-5: 180°	$F_x = -400; F_z = 0,1$
5-6: 225°	$F_x = -283; F_z = -283$
6-7: 270°	$F_x = 0,1; F_z = -400$
7-8: 315°	$F_x = 283; F_z = -283$

In the second part of the strength analysis, we had to determine deformations and stresses generated on the wheel after one turn. In this part of analysis, we had this boundary conditions: creating condition sequences so we could determine strength parameters after 45° rotation of the wheel (Tab.3.) with around 400N (force generated by quarter of the weight of whole structure of the robot); fixed support that was created on the created plane located on the plate of the wheel; surface to surface connection to connect all the parts of the wheel together.

IV. RESULT

The highest elemental stresses arose on the shaft, where the maximum values were around 3.5 MPa. The nodal stress reached around 5 MPa after averaging the result. The maximum deformation values were around 0.01 mm (Fig.3).

The resulting deformation on the wheel was minimal with maximum value of 0.006 mm and stresses, which according to calculation reached the value of 44 MPa. Based on origin and spreading of stress, we can state that bending was occurring, which means that calculation was successful (Fig.4).

Later we did analytical calculation of stress and deformation on a beam of aluminium profile of the base to determine, if the simulation was done correctly. We chose beam of aluminium profile with dimensions 93x47x680. The calculation was simplified and we considered simple rectangular cross-section with dimensions of 93x47. Two equally large forces of 250N were put on a beam (Fig.5.) and „a” represents third of a length of a beam. Initially it was necessary to solve reactions from static equilibrium conditions and to determine the course of moments and forces of this beam. Resulting stress of the analytical calculation was 1.5 MPa and maximum deformation was around 0.08mm. Values of deformations and stresses calculated by analytical calculations were very similar which means the simulation was done correctly.

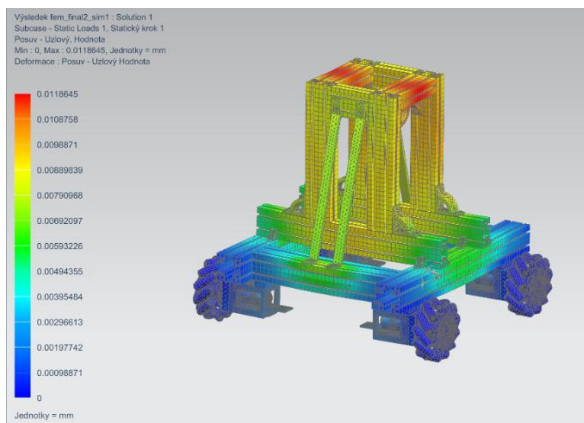


FIGURE 3: Deformations of the base

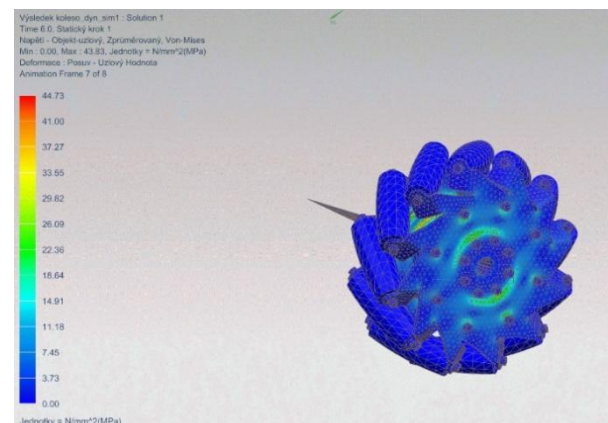


FIGURE 4: Stresses on the wheel

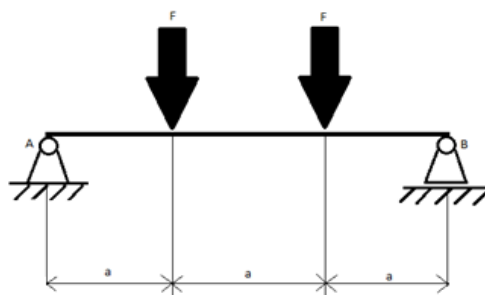


FIGURE 5: The selected beam of the mobile base used for analytical calculation

V. DISCUSSION

Based on the obtained results, we can state that in terms of strength, the base corresponds to the loading conditions that were generated by weight of the robot which is approximately 80 kilograms. The yield strength of each material used in the base is significantly higher than the stresses that were generated on the whole structure of the base. Later we created technical drawings for the construction of the individual parts, which were sent to the University in SIGMA in Clermont-Ferrand by which they will build the base.

VI. CONCLUSION

The main task of this work was to create a mobile base for a robot Baxter. At the beginning, there was created a first model of a base which was later modified so that the size and a weight was similar to the commercial base. It was also a priority to save money by creating this mobile base for a robot, as a price of a commercial base for a robot is approximately \$40,000 and more. The total cost of this base was around 5,000 €, which saved us a lot of money. This work can of course be continued. Its continuation would be programming the whole system into motion, where for example joystick would be used to control the base itself. Since the base uses simple parts of the drive axle and the question of turning is solved by unidirectional wheel, the mobility can be improved by turning the front wheels as in automobiles.

ACKNOWLEDGEMENTS

This paper was written with the financial support of the granting agency VEGA within the project solution No. 1/0108/19 and No. 1/0626/20 and of the granting agency KEGA within the project solution No. 005TUKE-4/2019.

REFERENCES

- [1] Smrček, Juraj; Kárník, Ladislav. Robotika Servisné roboty Navrhovanie, konštrukcia, riešenia, Strojnícka fakulta Technická univerzita v Košiciach 2008.
- [2] Murín, Justín; Hrabovský, Juraj; Kutiš, Vladimír. Metóda Konečných Prvkov Vybrané kapitoly pre mechatronikov, Slovenská technická univerzita v Bratislave 2014.
- [3] Matej, Jaroslav; Bodnár, Ferdinand. Simulácia virtuálnych prototypov- napät'ovo-deformačné analýzy, Technická univerzita vo Zvolene 2015.
- [4] Ravínger, Ján. Numerical methods in theory of structures, Slovenská technická univerzita v Bratislave 2014.
- [5] Vachálek, Ján; Takács, Gergely. Robotika, Slovenská technická univerzita v Bratislave 2014.
- [6] "Baxter – Redefining Robotics and Manufacturing – Rethink Robotics". Rethink Robotics. Archived from the original on 2014-08-26. Retrieved 2013-09-10.
- [7] "Four-legged Robot, 'Cheetah,' Sets New Speed Record". Reuters. 2012-03- 06. Archived from the original on 2013-10-22. Retrieved 2013-10-05.
- [8] Knight, Will (September 18, 2012). "This Robot Could Transform Manufacturing". MIT Technology Review.
- [9] Types of robots. <https://robots.ieee.org/learn/types-of-robots/>.



AD Publications

**Sector-3, MP Nagar, Bikaner,
Rajasthan, India**

www.adpublications.org, info@adpublications.org